Heliyon 10 (2024) e34474

Contents lists available at ScienceDirect

Heliyon

journal homepage: www.cell.com/heliyon

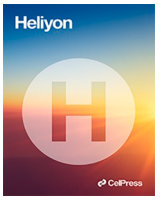

Research article

Identification of a prognosis-related phagocytosis regulator gene signature in medulloblastoma

Guoqing Han [a,b,1], Xingdong Wang [b,1], Ke Pu [c], Zhenhang Li [c], Qingguo Li [a,c,**], Xiaoguang Tong [b,c,*]

[a] Department of Neurosurgery, Tianjin University Huanhu Hospital, Tianjin, China
[b] Clinical College of Neurology, Neurosurgery and Neurorehabilitation, Tianjin Medical University, Tianjin, China
[c] Department of Neurosurgery, Tianjin Huanhu Hospital, Tianjin, China

ARTICLE INFO

Keywords:
Medulloblastoma
Phagocytosis
Prognosis
Gene signature
Gene expression

ABSTRACT

Objectives: The aims of this study were to screen for phagocytosis regulator-related genes in tissue samples from children with medulloblastoma (MB) and to construct a prognostic model based on those genes.

Methods: Differentially expressed genes between the MB and control groups were identified using the GSE50161 dataset from the Gene Expression Omnibus database. Prognosis-related phagocytosis regulator genes were selected from the GSE85217 dataset. Intersecting genes of the two datasets (differentially expressed prognosis-related phagocytosis regulator genes) were submitted to unsupervised cluster analysis to identify disease subtypes, after which the association between the subtypes and the immune microenvironment was analyzed. A prognostic risk score model was constructed, and functional, immune-related, and drug sensitivity analyses were performed.

Results: In total, 23 differentially expressed prognosis-related phagocytosis regulator genes were identified, from which two disease subtypes (clusters 1 and 2) were classified. The prognoses of the patients in cluster 2 were significantly worse than those of the patients in cluster 1. The immune microenvironment differed significantly between the two subtypes. Finally, 10 genes (*FAM81A*, *EZR*, *NDUFB9*, *RCOR1*, *FOXO4*, *NHLRC2*, *KIF23*, *PTPN6*, *SMAGP*, and *MED13*) were selected to establish the prognostic risk score model. The prognosis in the low-risk group was better than that in the high-risk group. The model genes *NDUFB9* and *PTPN6* were positively correlated with M2 macrophages.

Conclusion: Ten key phagocytosis regulator genes were screened to construct a prognostic model for MB. These genes may serve as key biomarkers for predicting the prognosis of patients with this type of brain cancer.

1. Introduction

Medulloblastoma (MB) is the most common type of malignant brain tumor in children, with an annual incidence of approximately

* Corresponding author. Department of Neurosurgery, Tianjin Huanhu Hospital, Tianjin, China.
** Corresponding author. Department of Neurosurgery, Tianjin University Huanhu Hospital, Tianjin, China.
E-mail addresses: lqg369@126.com (Q. Li), tongxiaoguanghhh@163.com (X. Tong).
[1] Guoqing Han and Xingdong Wang should be regard as co-first authors.

https://doi.org/10.1016/j.heliyon.2024.e34474
Received 30 January 2024; Received in revised form 9 July 2024; Accepted 10 July 2024
Available online 10 July 2024

five cases per 1 million individuals. The median diagnostic age of the patients is six years [1]. MBs are heterogeneous tumors that include four major subtypes: wingless/integrated (WNT), sonic hedgehog (SHH), Group 3 (G3), and Group 4 (G4) [2]. According to 2015 statistical data, the 10-year survival rate for MB has increased to 65 %, likely as a result of advances in treatment [3]. However, approximately 40 % of the patients develop metastatic and recurrent disease, which is the leading cause of death. Patients who survive suffer serious long-term side effects, such as neurocognitive deficits as well as auditory, visual, and other neurosensory disorders [4]. Thus, understanding the molecular mechanisms involved in the pathogenesis of MB and exploring possible biomarkers may help toward the development of more effective treatments for the disease.

The cancer niche depends on the inflammatory cells [45], with macrophages playing an important role in tumor inflammation. Tumor-associated macrophages support the growth of malignant cells through protective immunity, promoting tumor stem cell growth, and paving the route for metastasis [5,46]. Meningeal macrophages have been shown to suppress the initiation of mouse MB by inhibiting chemokine signaling in pre-tumor cells [6]. Macrophage-centered therapies include techniques that trigger the phagocytosis or extracellular death of tumor cells [7–9]. As a key macrophage function, phagocytosis enhances the oxidative metabolic profile and fosters an immunosuppressive phenotype in tumor-associated macrophages [10]. The phagocytic function of tumor-associated macrophages is a crucial determinant of tumor progression [11]. Reportedly, targeting macrophage phagocytosis is an effective antitumor strategy [12,13]. Gholamin et al. [14] also reported that the use of anti-CD47 antibodies to suppress the CD47 signaling pathway and allow for macrophage phagocytosis is effective against various adult cancers. However, reports on the role of macrophage-mediated phagocytosis in MB in children are limited. Furthermore, the regulatory mechanisms by which macrophage phagocytosis influences the progression and prognosis of MB remain largely unknown.

In this study, we screened phagocytosis regulator-related genes in tissue samples from children with MB and constructed a prognostic model on the basis of those genes. To this end, we downloaded MB-related datasets from the Gene Expression Omnibus (GEO) database and searched for phagocytosis regulator-related genes reported in the literature. On the basis of the identified phagocytosis regulator-related genes, a prognostic risk score (RS) model was constructed, following which functional and immune-related analyses were performed. The aims of this study were to screen phagocytosis regulator-related genes in children with MB and to construct a prognostic model based on those genes in order to reveal the key molecular mechanisms of macrophage phagocytosis in MB progression and provide promising biomarkers for predicting the disease prognosis.

2. Methods

2.1. Acquisition and preprocessing of gene expression data

Two datasets (GSE85217 and GSE50161) were downloaded from the GEO database. From GSE85217, MB samples from patients younger than 18 years of age were selected, whereupon 545 samples were retained as the training dataset. The GPL22286 [Hugene-1101-st] Affymetrix Human Gene 1.1 ST Array [HuGene11stv1_Hs_ENSG version 19.0.0] platform was used for the analysis. GSE50161, which provides data on 22 children with MB and 13 healthy (control) individuals, was used to identify differentially expressed genes (DEGs), with the GPL570 [HG-U133_Plus_2] Affymetrix Human Genome U133 Plus 2.0 platform used for this analysis.

2.2. Acquisition of phagocytosis regulator-related genes

In total, 266 phagocytosis regulator-related genes were obtained from the literature search [15].

2.3. Screening of phagocytosis regulator genes related to prognosis

The 530 MB samples selected from GSE85217 had an overall survival (OS) of more than 0. Univariate Cox regression analysis of the phagocytosis regulator genes was carried out using survival 2.41 [16], and the results were combined with the clinical survival and prognosis information of the 530 MB samples to select phagocytosis regulator genes that were significantly related to OS prognosis. Statistical significance was set at a P-value of less than 0.05.

2.4. Differentially expressed gene selection

The DEGs between the MB and control groups in GSE50161 were analyzed using linear regression and the empirical Bayes method provided in Limma 3.10.3. Corresponding P-values and log fold changes (FC) in gene expression levels were obtained. Additionally, the Benjamini–Hochberg method was applied for multiple testing correction, and the adjusted P-value was obtained. The thresholds of DEGs were set as an adjusted P-value of less than 0.05 and a $|\log2\ FC|$ value greater than 0.585.

2.5. Protein–protein interaction network construction

The DEGs and prognosis-related phagocytosis regulator genes were compared, and the intersecting genes were considered as differentially expressed prognosis-related phagocytosis regulator genes. The interactions among these genes were analyzed using STRING version 11.5 [17]. The protein–protein interaction (PPI) score was set at 0.15.

2.6. Identification of disease subtypes

On the basis of the expression levels of the differentially expressed prognosis-related phagocytosis regulator genes in the tumor samples, Pearson's correlation coefficient-based hierarchical cluster analysis was performed on the patients in GSE85217 using ConsensusClusterPlus version 1.58.0 [18]. Then, survival prognostic correlations between the different disease subtypes were assayed using the Kaplan–Meier curve method in the survival package. Subsequently, the clinical information of the samples belonging to the different subtypes was compared.

2.7. Association of the disease subtype with the immune microenvironment

On the basis of the expression matrix of all genes, the relative infiltration abundance of the 22 types of immune cells in each sample was estimated using CIBERSORT software [19]. Differences in the proportions of immune cell types among the different subtypes were then compared. Additionally, the ESTIMATE algorithm [20] was used to estimate the stromal and immune scores of the tumor samples on the basis of the expression data. The two scores were added to produce a score that could be used to estimate the tumor purity. Differences in immune, stromal, and microenvironmental scores and tumor purity were compared between the two subtypes.

Moreover, on the basis of their expression levels in the disease samples, the specific immune checkpoint genes were extracted, including *PD1* (PDCD1), *PD-L1* (CD274), *CTLA-4* (CTLA4), *CD278* (ICOS), *LAG3*, *CD73*, *Tim3* (HAVCR2), *CD47*, *TIGIT*, *myd1* (SIRPA), *BTLA*, *4*-1BB (TNFRSF9), *OX40* (TNFRSF4), and *B7–H4* (VTCN1). Additionally, the expression of HLA family genes was determined. Differences in expression levels between the two disease subtypes were then compared.

2.8. Construction and validation of the prognostic model

On the basis of the expression levels of the differentially expressed prognosis-related phagocytosis regulator genes in each sample, the disease samples were randomly grouped into training and validation sets (1:1) together with their survival information. The optimal gene combination was further screened using the stepwise regression model of the glmnet package (version 2.0–18) in R3.6.1 [21]. On the basis of the LASSO regression coefficient of the gene combination and expression levels of genes in the GSE85217 samples, the following RS model was constructed:

$$RS = \sum \beta_{gene} \times Exp_{gene}$$

Where β_{gene} represents the LASSO regression coefficient of the gene, and Exp_{gene} represents the gene expression level in the GSE85217 sample.

Next, the GSE85217 samples in the training and verification sets were divided into high- ($RS \geq$ RS median value) and low-risk ($RS <$ RS median value) groups according to the RS median values. The Kaplan–Meier curve method in survival 2.41–1 was used to assess the association between risk grouping and actual survival information.

2.9. Nomogram establishment

Univariate Cox regression analysis was performed for RS, age, MetS status, and sex to evaluate whether the above RS model served as an independent prognostic factor. Variables with a P-value of less than 0.05 were included in the multivariate Cox regression analysis. The obtained variables were then used to construct a nomogram to predict one-, three-, and five-year survival. Simultaneously, a correction curve was drawn to verify the accuracy of the model.

2.10. Gene set enrichment analysis among different risk groups

Gene set enrichment analysis (GSEA) was performed with Kyoto Encyclopedia of Genes and Genomes (KEGG) and Gene Ontology (GO) datasets using the clusterProfiler package in the MSigDB v7.4 database [22]. The threshold was set at an adjusted P-value of less than 0.05.

2.11. Correlation between model genes and immune cell infiltration

The proportion of the 22 immune cells in each sample was determined using CIBERSORT software [19]. The relationship between the 22 immune cells and the prognostic model genes was analyzed using Spearman's rank-order correlation analysis. Genes that correlated with macrophages were selected and displayed on a heatmap.

2.12. Correlation between risk grouping and drug sensitivity

Using the pRRophetic algorithm, a ridge regression model was constructed to predict the IC_{50} of 39 common drugs on the basis of the Genomics of Drug Sensitivity in Cancer cell line and gene expression profiles. The Wilcoxon test was used to determine whether there were significant differences in the IC_{50} values of each drug between the different disease subtypes.

3. Results

3.1. Prognosis-related phagocytosis regulator gene screening

In GSE50161, there were 3293 downregulated and 3461 upregulated DEGs between the MB and control groups. The volcano plot is shown in Fig. 1A. Based on the gene expression levels and survival information from the GSE85217 dataset, univariate Cox regression analysis of the 266 phagocytosis regulator-related genes identified 59 genes that were significantly associated with MB prognosis ($P < 0.05$; Fig. 1B).

The intersection of the DEGs and prognosis-related phagocytosis regulator genes revealed 23 genes in common, which were considered the differentially expressed prognosis-related phagocytosis regulator genes (Fig. 1C). A PPI network was then constructed that included 14 proteins and 17 interaction pairs (Fig. 1D).

3.2. Disease subtype analysis

Based on the expression levels of the 23 differentially expressed prognosis-related phagocytosis regulator genes in the disease samples, two disease subtypes were obtained after consistent cluster analysis (Fig. 2A). A heatmap of the expression levels of the 23 genes in the two subtypes is shown in Fig. 2C. Survival analysis revealed that the prognoses of the patients in cluster 2 were significantly worse than those of the patients in cluster 1 (Fig. 2B). Moreover, the phagocytosis regulator score of cluster 1 was significantly higher than that of cluster 2 (Fig. 2D). Additionally, the clinical factors of the two subtypes were compared, and a significance test was conducted, as shown in Table 1. Significant differences with regard to sex and MetS status were observed between the two subtypes.

3.3. Association of the disease subtypes with immunity

Of the 22 immune cell types, nine (viz., memory B cells, naïve $CD4^+$ T cells, resting $CD4^+$ memory T cells, regulatory T cells,

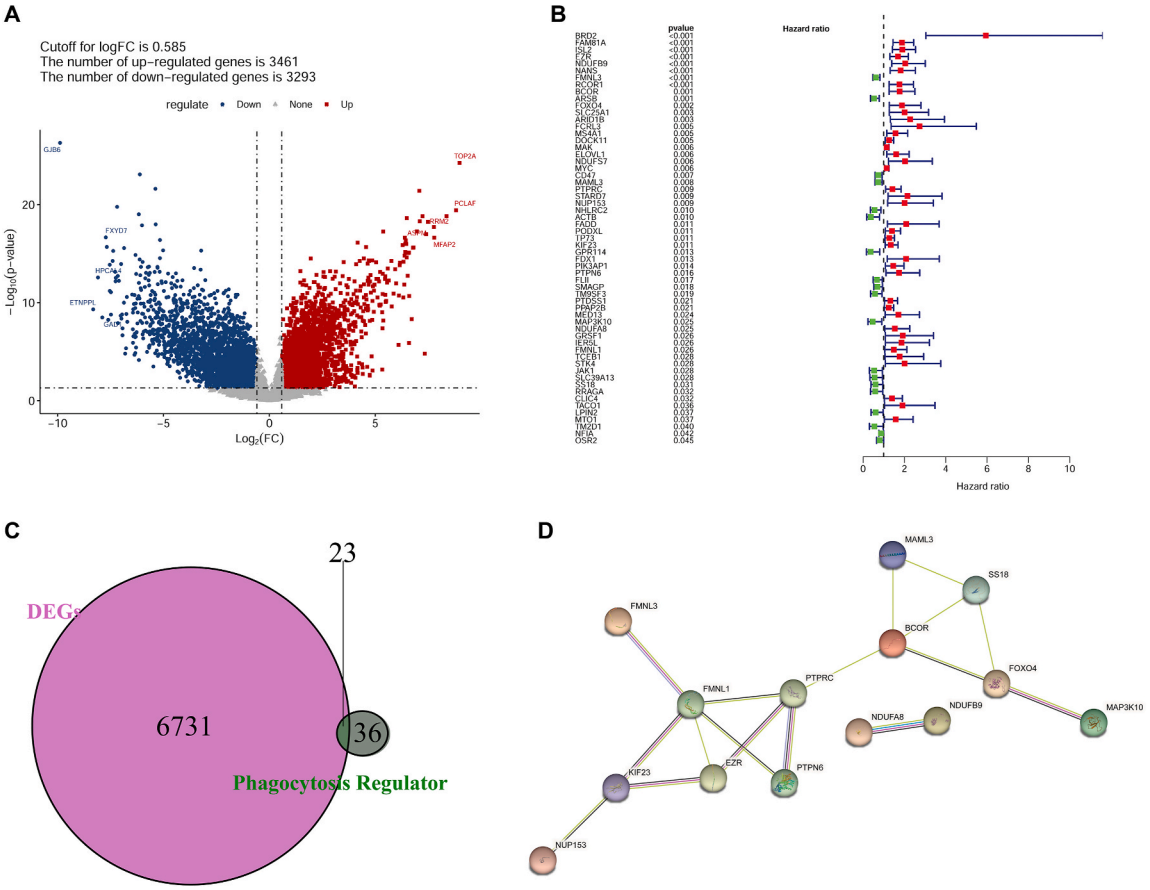

Fig. 1. A, Volcano plot of differentially expressed genes (DEGs). Red represents upregulated genes, and blue represents downregulated genes. B, Univariate Cox regression analysis of phagocytosis regulator-related genes. C, Venn diagram of DEGs and phagocytosis regulator-related genes. D, Protein–protein interaction network of the phagocytosis regulator-related DEGs.

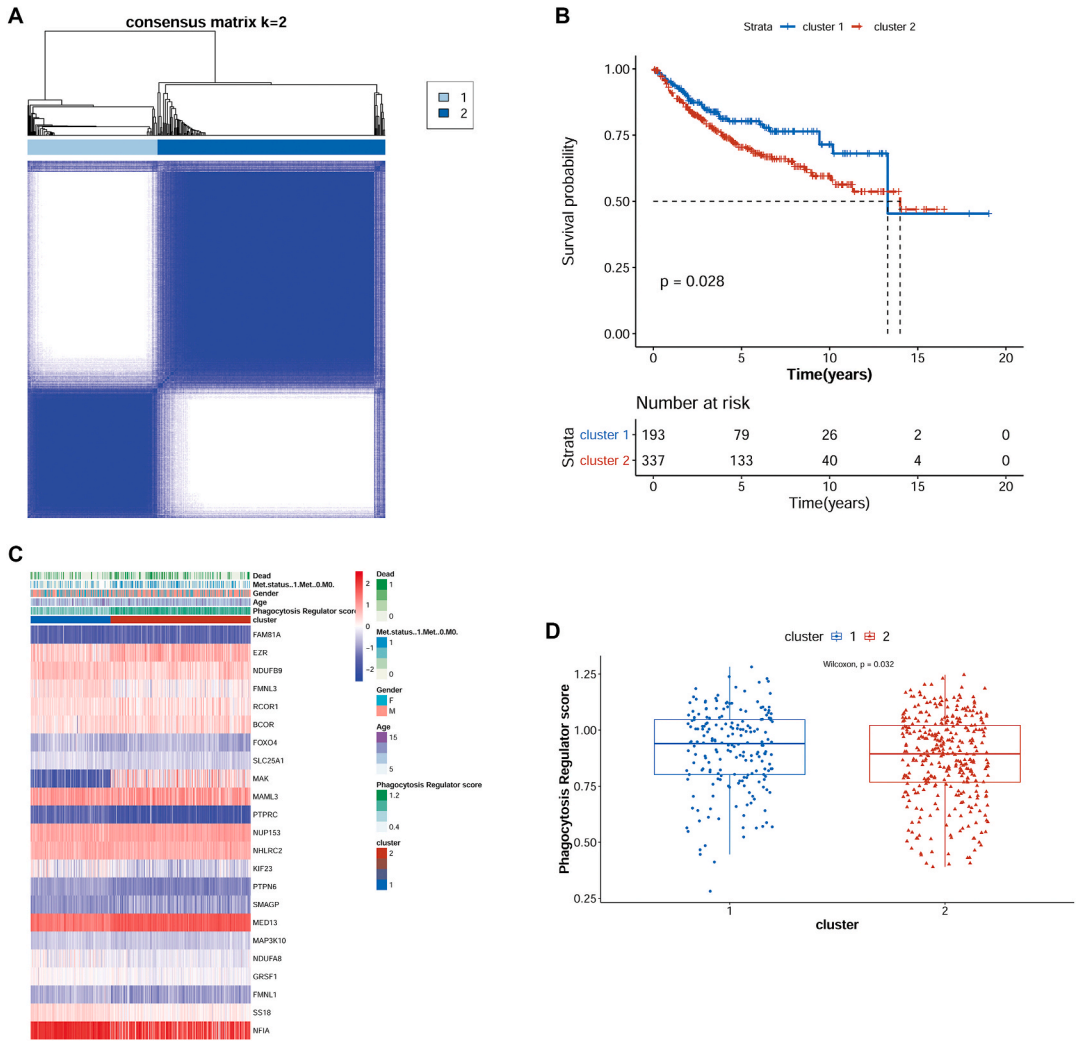

Fig. 2. A, Results of cluster analysis of the differentially expressed phagocytosis regulator-related genes. B, Kaplan–Meier survival curves of the two disease subtypes. C, Heatmap of prognosis-related phagocytosis regulator gene expression in the two subtypes. D, Phagocytosis regulator scores of the two subtypes.

Table 1
Statistical table of clinical information for two subtypes.

	cluster 1 (N = 198)	cluster 2 (N = 347)	P-value
Gender			
F	83.0 (41.9 %)	106 (30.5 %)	0.00969
M	114 (57.6 %)	239 (68.9 %)	
Missing	1.00 (0.5 %)	2.00 (0.6 %)	
Age (years)			
Mean (SD)	7.20 (4.80)	7.59 (3.57)	0.318
Median [Min, Max]	7.00 [0.240, 17.2]	7.21 [1.25, 17.3]	
Met.status			
0	131 (66.2 %)	195 (56.2 %)	<0.001
1	37.0 (18.7 %)	125 (36.0 %)	
Missing	30.0 (15.2 %)	27.0 (7.8 %)	
Dead			
0	157 (79.3 %)	241 (69.5 %)	0.0169
1	41.0 (20.7 %)	106 (30.5 %)	

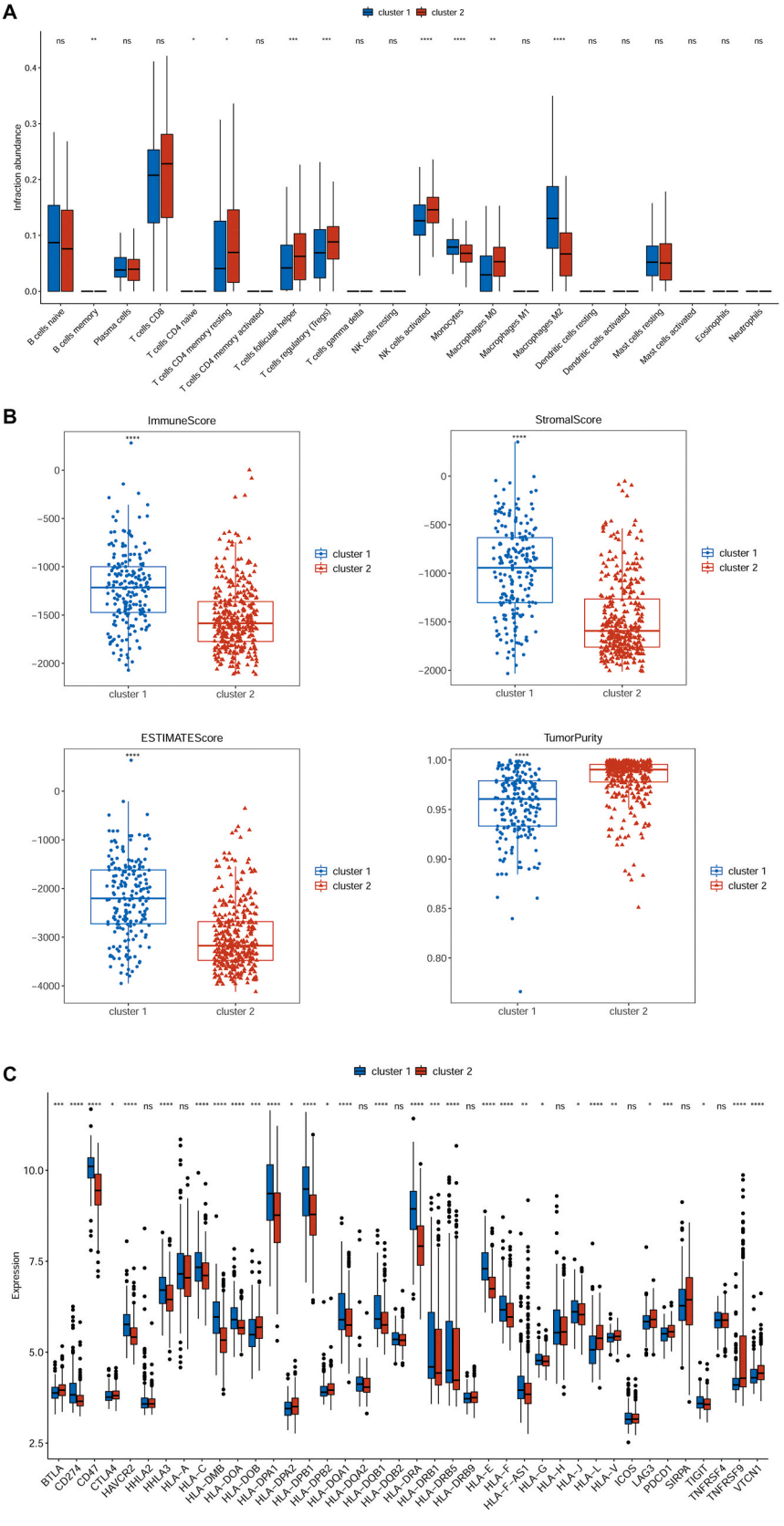

(caption on next page)

Fig. 3. A, Relative infiltration of the 22 immune cell types in the two disease subtypes. B, Box plots of the immune, stromal, and immune microenvironment scores, and tumor purity of the two subtypes. C, Expression of immune checkpoint and HLA family genes in the two subtypes.

follicular helper T cells, monocytes, activated natural killer cells, M0 macrophages, and M2 macrophages) showed markedly different relative infiltration levels between the two disease subtypes (Fig. 3A). Further comparisons between the two subtypes revealed that the stromal and immune score estimates were significantly lower in cluster 2 than in cluster 1, but the tumor purity was significantly higher in cluster 2 (Fig. 3B).

The differences in expression of specific immune checkpoint and HLA family genes between the two subtypes are shown in Fig. 3C. Most genes showed significantly different expression levels between the two subtypes.

3.4. Construction and validation of the prognostic model

On the basis of the 23 differentially expressed prognosis-related phagocytosis regulator genes, 10 optimal genes (*FAM81A*, *EZR*, *NDUFB9*, *RCOR1*, *FOXO4*, *NHLRC2*, *KIF23*, *PTPN6*, *SMAGP*, and *MED13*) were screened using a stepwise regression algorithm. The RS model was established using the regression coefficients of these 10 optimal genes and their expression levels in the samples from the training set. The samples were divided into high- and low-risk groups for both the training and validation sets. The prognosis of the low-risk group was significantly better than that of the high-risk group (Fig. 4A and B). The proportion of each disease subtype in the two risk groups was calculated to determine the relationship between the risk grouping and subtypes. As shown in Fig. 4C, the high-risk group contained more samples from cluster 2, which had a poor prognosis.

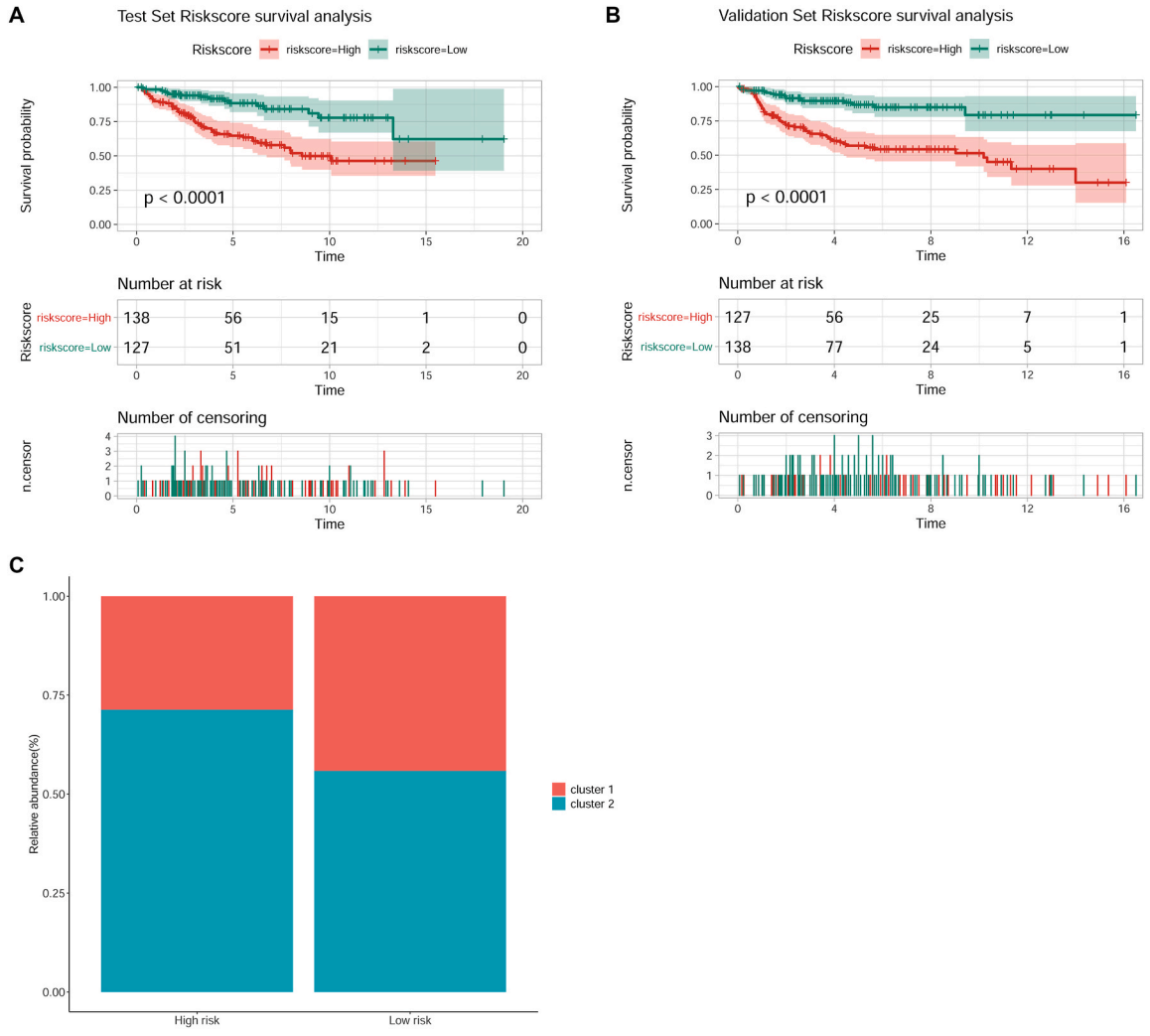

Fig. 4. A and B, Prognostic Kaplan–Meier curves based on the risk score model for the training (A) and validation sets (B). C, Histogram of the proportions of the two disease subtypes in the high- and low-risk groups.

3.5. Independence analysis and nomogram establishment

The RS, MetS status, and disease cluster were found to be independent prognostic factors of OS, according to the univariate Cox regression analysis ($P < 0.05$) (Fig. 5A). After multivariate Cox regression analysis, the RS and MetS status were retained as independent prognostic factors (Fig. 5B) and used to construct a nomogram for predicting one-, three-, and five-year survival (Fig. 5C). The "total points" axis in the first row was used to predict the survival of the samples by integrating various clinical indicators. The predicted one-, three-, and five-year survival rates were in accordance with the actual survival rates (Fig. 5D).

3.6. Gene set enrichment analysis

GSEA was performed for all genes in the two risk groups, whereupon they were found to be enriched in 414 GO terms and 24 KEGG pathways. The genes related to DNA replication, ribosomes, spliceosomes, and chronic myeloid leukemia were upregulated, whereas those associated with axon guidance and the calcium and WNT signaling pathways were downregulated (Fig. 6A). Additionally, genes enriched in spindle elongation and mitotic DNA replication processes were activated, whereas those related to the regulation of *trans*-synaptic signaling and metal and calcium ion transport were suppressed (Fig. 6B).

3.7. Correlation between the model genes and immune cell infiltration

Spearman's correlation analysis revealed that M2 macrophages were positively correlated with *NDUFB9* and *PTPN6* expression (Fig. 7A). The correlation scatter plots are shown in Fig. 7B.

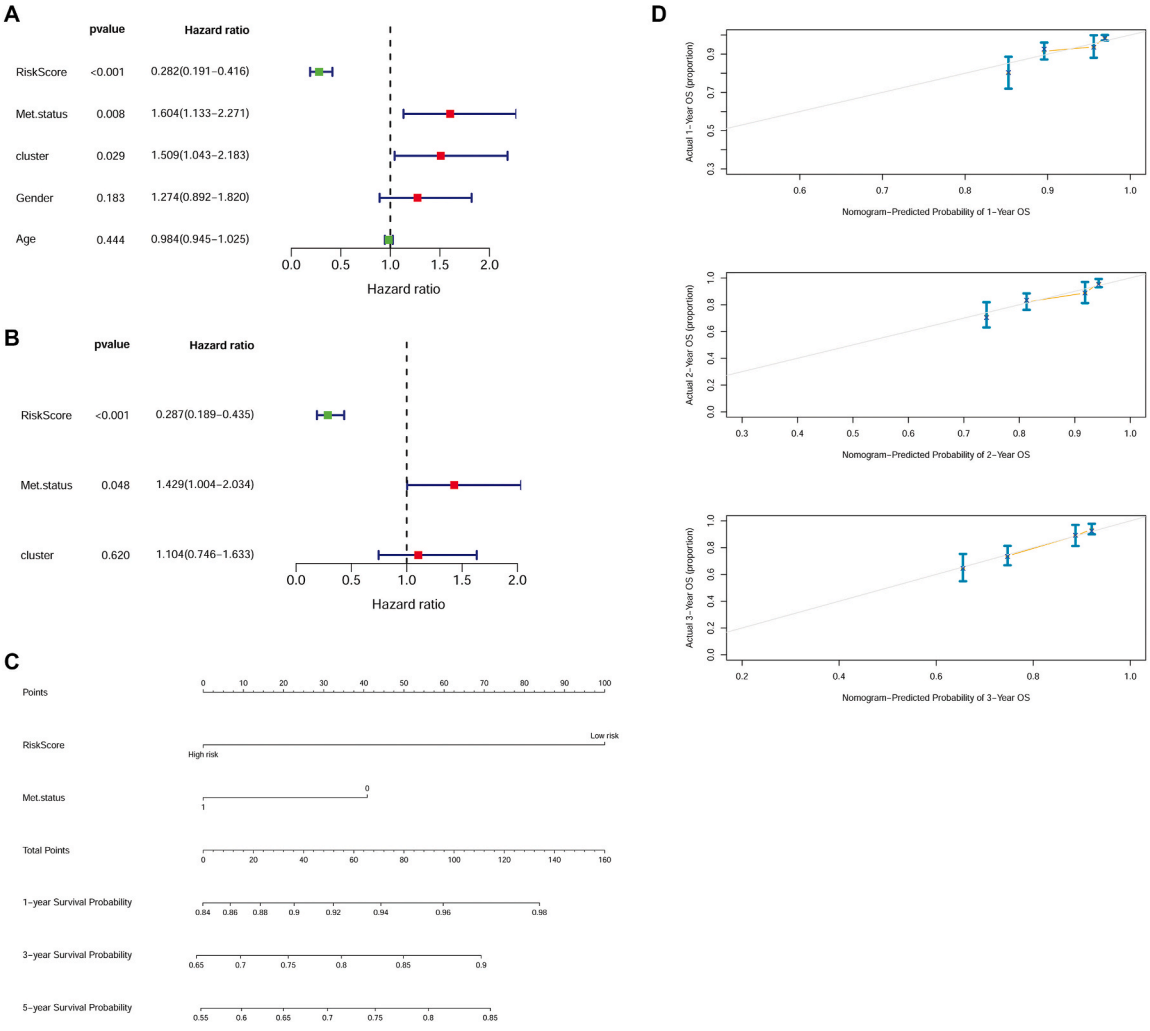

Fig. 5. A and B, Univariate (A) and multivariate (B) Cox regression forest maps of clinical factors. C, Nomogram used to predict the one-, three-, and five-year survival rates. D, Consistency charts of the predicted and actual survival rates. The horizontal axis represents the predicted survival rate.

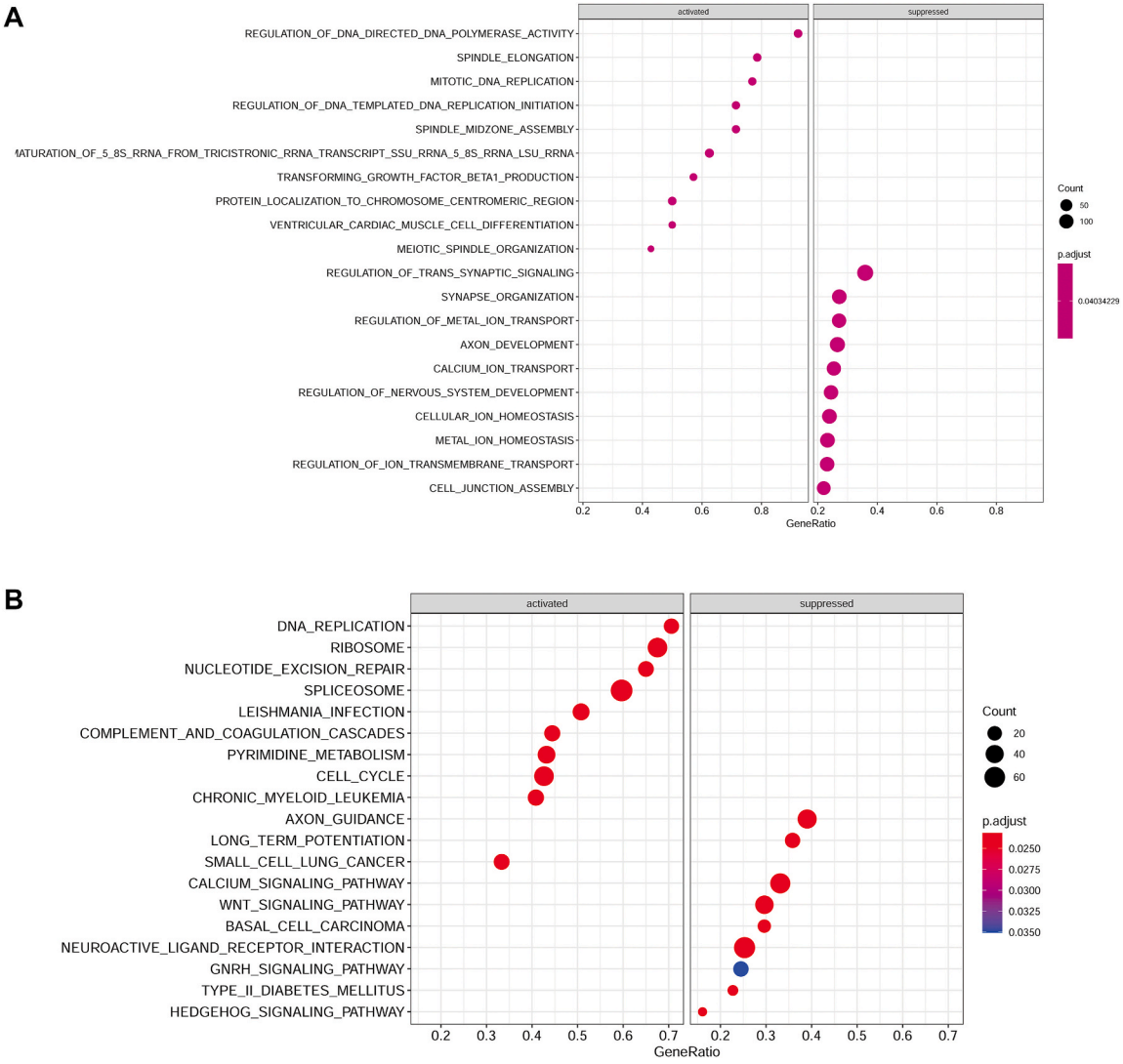

Fig. 6. GO (A) and KEGG pathway maps (B) obtained by means of GSEA.

3.8. Correlation between risk grouping and drug sensitivity

The IC_{50} values of the common drugs were predicted using the pRRophetic algorithm. Nine drugs (AZD6244, AP.24,534, axitinib, bryostatin.1, FTI.277, erlotinib, bicalutamide, AS601245, and CMK) showed significant differences in IC_{50} values between the two risk groups (Fig. S1).

4. Discussion

In this study, 23 differentially expressed prognosis-related phagocytosis regulator genes in MB were selected, and two disease subtypes were identified on the basis of those genes. The prognoses of the patients in cluster 2 were significantly worse than those of the patients in cluster 1. Moreover, the immune microenvironment differed significantly between the two subtypes. Finally, 10 genes were selected using a stepwise regression algorithm to establish a prognostic model. The prognosis in the low-risk group was significantly better than that in the high-risk group. Furthermore, the model genes *NDUFB9* (encoding NADH:ubiquinone oxidoreductase subunit B9) and *PTPN6* (encoding protein tyrosine phosphatase non-receptor type 6) were positively correlated with M2 macrophages.

Innate immunity is a major part of the human immune system and serves as the first line of defense against infectious agents and malignant tumors [23]. Additionally, the innate immune system can cross-initiate the adaptive immune system, in which antigens are presented to naïve B and T cells by antigen-presenting cells [24]. The precursor to this bridge between innate and adaptive immunity is the capture of antigen-presenting cells via phagocytosis [25]. Therefore, understanding the mechanisms underlying phagocytosis

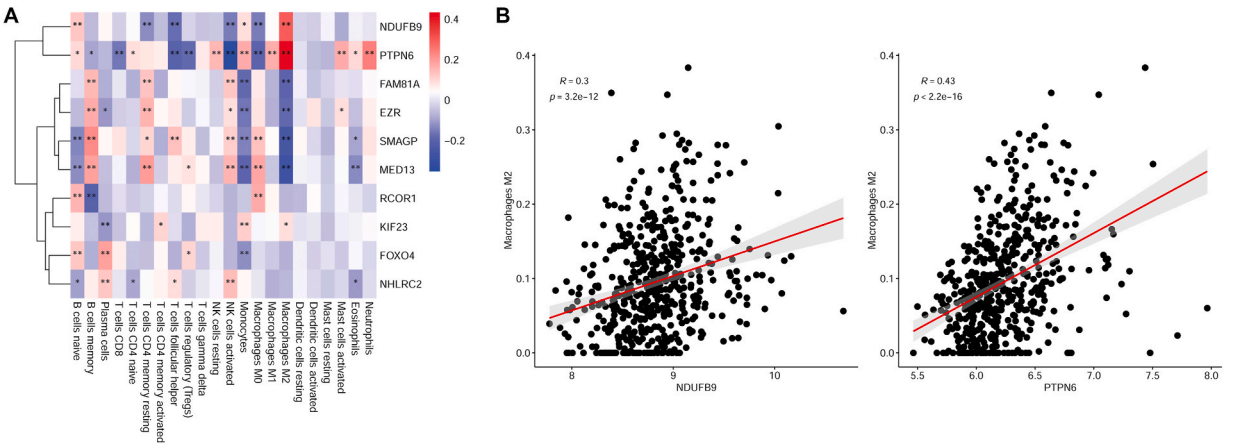

Fig. 7. A, Spearman's rank-order correlations between the model genes and immune cells (*P < 0.05, **P < 0.01, ***P < 0.001). B, Scatter plots of the correlations between M2 macrophages and the *NDUFB9* and *PTPN6* genes.

regulation can provide novel avenues for the development of next-generation therapeutic methods that act to unleash the power of the innate immune system, particularly macrophages [26]. In this study, 23 differentially expressed prognosis-related phagocytosis regulator genes in MB were selected on the basis of an MB-related dataset and phagocytosis regulator gene sets reported in the literature. These genes may serve as phagocytosis regulators during MB treatment.

Molecular profiling of MB has identified at least four molecular subtypes (WNT, SHH, G3, and G4, the last two being non-Wnt/non-SHH), which have different clinical manifestations and prognoses [27]. The stratification of MB into subtypes has important clinical implications, as identifying their oncogenic drivers may lead to subtype-specific targeted therapy [28] and de-escalation strategies to treat tumors, resulting in better prognosis [29]. In this study, the MB samples were clustered into two subtypes (clusters 1 and 2) on the basis of the 23 differentially expressed prognosis-related phagocytosis regulator genes. Because the patients in cluster 2 were found to have a significantly worse prognosis, de-escalation strategies for the treatment of patients with this specific disease subtype may be feasible. Moreover, the immune and stromal scores in cluster 1 were significantly higher than those in cluster 2, suggesting that the patients in cluster 1 may be more suitable for immunotherapy.

Among the 10 genes (*FAM81A*, *EZR*, *NDUFB9*, *RCOR1*, *FOXO4*, *NHLRC2*, *KIF23*, *PTPN6*, *SMAGP*, and *MED13*) used to construct the RS model, *NDUFB9* and *PTPN6* were found to be positively correlated with M2 macrophages. As members of innate immunity, macrophages are involved in antigen presentation and phagocytosis. After differentiating from monocyte precursors, macrophages polarize toward the M1 or M2 phenotype [30]. It has been reported that macrophage polarization plays a key role in the development of brain tumors, including MB [31,32]. NDUFB9 is an accessory component of the mitochondrial membrane respiratory chain. Its reduced expression promotes breast cancer cell proliferation and metastasis [33]. Lin et al. demonstrated that *NDUFB9* might play a role in determining the malignancy or benignity of brain neoplasms through its modulation of mitochondrial metabolism [34]. PTPN6 is a crucial regulatory protein that plays a central role in cellular signal transduction pathways involved in the regulation of inflammation and cell death [35]. *PTPN6* has been shown to exert immunosuppressive effects on glioblastomas [36]. Given the roles of *NDUFB9* and *PTPN6* in cancer development, we speculate that both genes may be associated with the prognosis of MB through their relationship with M2 macrophages.

Several of the other eight genes have been reported to be associated with MB. Ezrin (EZR) is a cytoplasmic peripheral protein that cross-links the oncogenic dry marker CD44 and cytoskeletal markers that participate in the migration of MB cells [37]. *EZR* knockdown reduces the migratory, adhesive, and invasive abilities of MB cells [38]. *RCOR1* encodes REST corepressor 1 (CoREST), which acts as a core scaffold for recruiting epigenetic remodelers and DNA-binding factors. The post-translational modification of CoREST is a novel molecular mechanism associated with the G3 and G4 subtypes of MB [39]. Missense mutations in *MED13* (which encodes mediator complex subunit 13) were detected in the WNT subtype of MB [40]. Despite limited reports on the involvement of the other genes in MB, they have been shown to play key roles in other cancers. For instance, Forkhead box protein O4 (FOXO4) suppresses the migration and metastasis of colorectal cells [41]. High expression of the protein NHL repeat containing 2 (NHLRC2) is associated with shortened survival in lung adenocarcinoma [42]. Kinesin family member 23 (KIF23) contributes to the deterioration of nasopharyngeal carcinoma through modulation of the WNT/β-catenin signaling pathway [43]. Overexpression of small cell adhesion glycoprotein (SMAGP) fosters the malignant characteristics of glioblastoma cells [44]. Taken together, these findings suggest that these 10 model genes could serve as key prognostic factors in MB.

This study had some limitations. First, the sample size was small. Second, the roles and regulatory mechanisms of these key genes in MB development have not been validated through *in vivo* or *in vitro* experiments. Therefore, additional samples need to be collected to verify our results.

5. Conclusion

This study identified two MB subtypes on the basis of 23 differentially expressed prognosis-related phagocytosis regulator genes. Additionally, 10 key phagocytosis regulator genes were used to establish a prognostic model for MB. These 10 genes may serve as key prognostic biomarkers for this brain cancer type.

Funding

This work was supported by Tianjin Science and Technology Planning Project (Program No. 21JCZDJC00460).

Ethics approval and consent to participate

Our analyses were conducted using publicly available data approved by the relevant review boards. Therefore, no additional ethical approval or consent was required for this study.

Data availability

The data supporting the findings of this study are available from the corresponding author upon reasonable request.

CRediT authorship contribution statement

Guoqing Han: Writing – original draft. **Xingdong Wang:** Investigation. **Ke Pu:** Investigation. **Zhenhang Li:** Project administration. **Qingguo Li:** Validation. **Xiaoguang Tong:** Writing – review & editing, Conceptualization.

Declaration of competing interest

The authors declare that they have no known competing financial interests or personal relationships that could have appeared to influence the work reported in this paper.

Acknowledgements

Not applicable.

Appendix A. Supplementary data

Supplementary data to this article can be found online at https://doi.org/10.1016/j.heliyon.2024.e34474.

References

[1] Q.T. Ostrom, G. Cioffi, K. Waite, C. Kruchko, J.S. Barnholtz-Sloan, CBTRUS statistical report: primary brain and other central nervous system tumors diagnosed in the United States in 2014–2018, Neuro Oncol. 23 (2021) iii1–iii105.
[2] K. Juraschka, M.D. Taylor, Medulloblastoma in the age of molecular subgroups: a review: JNSPG 75th anniversary invited review article, J. Neurosurg. Pediatr. 24 (2019) 353–363.
[3] Q.T. Ostrom, H. Gittleman, G. Truitt, A. Boscia, C. Kruchko, J.S. Barnholtz-Sloan, CBTRUS statistical report: primary brain and other central nervous system tumors diagnosed in the United States in 2011–2015, Neuro Oncol. 20 (2018) iv1–iv86.
[4] M. Chevignard, H. Câmara-Costa, F. Doz, G. Dellatolas, Core deficits and quality of survival after childhood medulloblastoma: a review, Neuro-Oncology Practice 4 (2017) 82–97.
[5] A. Christofides, L. Strauss, A. Yeo, C. Cao, A. Charest, V.A. Boussiotis, The Complex Role of Tumor-Infiltrating Macrophages, Nat. Immunol. 23 (2022) 1148–1156.
[6] N.T. Pokrajac, N.J. Tokarew, A. Gurdita, A. Ortin-Martinez, V.A. Wallace, Meningeal macrophages inhibit chemokine signaling in pre-tumor cells to suppress mouse medulloblastoma initiation, Dev. Cell. 58 (2023) 2015–2031. e8.
[7] H. Wang, X. Wang, X. Zhang, W. Xu, The promising role of tumor-associated macrophages in the treatment of cancer, Drug Resist. Updat. 73 (2024) 101041.
[8] Y. Wang, A. Barrett, Q. Hu, Targeting macrophages for tumor therapy, AAPS J. 25 (2023) 80.
[9] L. Zhou, T. Zhao, R. Zhang, C. Chen, J. Li, New Insights into the Role of Macrophages in Cancer Immunotherapy, Front Immunol. 15 (2024) 1381225.
[10] M.A. Gonzalez, D.R. Lu, M. Yousefi, A. Kroll, C.H. Lo, C.G. Briseño, J.V. Watson, S. Novitskiy, V. Arias, H. Zhou, A.P. Stapper, M.K. Tsai, E.L. Ashkin, C. W. Murray, C.M. Li, M.M. Winslow, K.V. Tarbell, Phagocytosis increases an oxidative metabolic and immune suppressive signature in tumor macrophages, J. Exp. Med. 220 (2023) e20221472.
[11] M. Lecoultre, V. Dutoit, P.R. Walker, Phagocytic function of tumor-associated macrophages as a key determinant of tumor progression control: a review, J. Immunother. Cancer 8 (2020) e001408.
[12] S. Chen, S.W. Lai, C.E. Brown, M. Feng, Harnessing and enhancing macrophage phagocytosis for cancer therapy, Front. Immunol. 12 (2021) 635173.
[13] S.Y. Li, Y.L. Guo, J.W. Tian, H.J. Zhang, R.F. Li, P. Gong, Z.L. Yu, Anti-tumor strategies by harnessing the phagocytosis of macrophages, Cancers (Basel) 15 (2023) 2717.
[14] S. Gholamin, S.S. Mitra, A.H. Feroze, J. Liu, S.A. Kahn, M. Zhang, R. Esparza, C. Richard, V. Ramaswamy, M. Remke, Disrupting the CD47-SIRPα anti-phagocytic axis by a humanized anti-CD47 antibody is an efficacious treatment for malignant pediatric brain tumors, Sci. Transl. Med. 9 (2017) eaaf2968.

[15] G. Qu, Y. Xu, Z. Lu, H. Nie, C. Tang, J. Hou, X. Wen, Prognostic signature development on the basis of macrophage phagocytosis-mediated oxidative phosphorylation in Bladder cancer, Oxid. Med. Cell. Longev. 29 (2022) 4754935.
[16] P. Wang, Y. Wang, B. Hang, X. Zou, J.H. Mao, A novel gene expression-based prognostic scoring system to predict survival in gastric cancer, Oncotarget 7 (2016) 55343–55351.
[17] D. Szklarczyk, A.L. Gable, D. Lyon, A. Junge, S. Wyder, J. Huerta-Cepas, M. Simonovic, N.T. Doncheva, J.H. Morris, P. Bork, STRING v11: protein–protein association networks with increased coverage, supporting functional discovery in genome-wide experimental datasets, Nucleic Acids Res. 47 (2019) D607–D613.
[18] M.D. Wilkerson, D.N. Hayes, ConsensusClusterPlus: a class discovery tool with confidence assessments and item tracking, Bioinformatics 26 (2010) 1572–1573.
[19] B. Chen, M.S. Khodadoust, C.L. Liu, A.M. Newman, A.A. Alizadeh, Profiling tumor infiltrating immune cells with CIBERSORT, Methods Mol. Biol. 1711 (2018) 243–259.
[20] K. Yoshihara, M. Shahmoradgoli, E. Martínez, R. Vegesna, H. Kim, W. Torres-Garcia, V. Treviño, H. Shen, P.W. Laird, D.A. Levine, S.L. Carter, G. Getz, K. Stemke-Hale, G.B. Mills, R.G.W. Verhaak, Inferring tumour purity and stromal and immune cell admixture from expression data, Nat. Commun. 4 (2013) 2612.
[21] J. Friedman, T. Hastie, R. Tibshirani, Glmnet: Lasso and Elastic-Net Regularized Generalized Linear Models, 2009.
[22] A. Liberzon, A. Subramanian, R. Pinchback, H. Thorvaldsdóttir, P. Tamayo, J.P. Mesirov, Molecular signatures database (MSigDB) 3.0, Bioinformatics 27 (2011) 1739–1740.
[23] L. Maiorino, J. Daßler-Plenker, L. Sun, M. Egeblad, Innate Immunity and Cancer Pathophysiology, Annu. Rev. Pathol. 17 (2022) 425–457.
[24] A. Iwasaki, R. Medzhitov, Regulation of adaptive immunity by the innate immune system, science 327 (2010) 291–295.
[25] P. Patel, S. Chatterjee, Innate and adaptive immunity: Barriers and receptor-based recognition, in: Immunity and Inflammation in Health and Disease, ̈eds, Elsevier, 2018, pp. 3–13.
[26] L. Cassetta, J.W. Pollard, Targeting macrophages: therapeutic approaches in cancer, Nat. Rev. Drug Discov. 17 (2018) 887–904.
[27] M.D. Taylor, P.A. Northcott, A. Korshunov, M. Remke, Y.-J. Cho, S.C. Clifford, C.G. Eberhart, D.W. Parsons, S. Rutkowski, A. Gajjar, Molecular subgroups of medulloblastoma: the current consensus, Acta Neuropathol. 123 (2012) 465–472.
[28] T. Sursal, J.S. Ronecker, A.J. Dicpinigaitis, A.L. Mohan, M.E. Tobias, C.D. Gandhi, M. Jhanwar-Uniyal, Molecular stratification of medulloblastoma: clinical outcomes and therapeutic interventions, Anticancer Res. 42 (2022) 2225–2239.
[29] T. Eisemann, R.J. Wechsler-Reya, Coming in from the cold: overcoming the hostile immune microenvironment of medulloblastoma, Genes & Development 36 (2022) 514–532.
[30] K.V. Myers, K.J. Pienta, S.R. Amend, Cancer cells and M2 macrophages: cooperative invasive ecosystem engineers, Cancer Control 27 (2020) 1073274820911058.
[31] E. Guadagno, I. Presta, D. Maisano, A. Donato, C.K. Pirrone, G. Cardillo, S.D. Corrado, C. Mignogna, T. Mancuso, G. Donato, Role of macrophages in brain tumor growth and progression, Int. J. Mol. Sci. 19 (2018) 1005.
[32] V. Maximov, Z. Chen, Y. Wei, M.H. Robinson, C.J. Herting, N.S. Shanmugam, V.A. Rudneva, K.C. Goldsmith, T.J. MacDonald, P.A. Northcott, Tumour-associated macrophages exhibit anti-tumoural properties in Sonic Hedgehog medulloblastoma, Nat. Commun. 10 (2019) 1–11.
[33] L.D. Li, H.F. Sun, X.X. Liu, S.P. Gao, H.L. Jiang, X. Hu, W. Jin, Down-regulation of NDUFB9 promotes breast cancer cell proliferation, metastasis by mediating mitochondrial metabolism, PLoS One 10 (2015) e0144441.
[34] J.C. Lin, Y.C. Wu, F.C. Yang, J.T. Tsai, D.Y. Huang, W.H. Liu, Genome-wide association study identifies multiple susceptibility Loci for malignant neoplasms of the brain in Taiwan, J. Pers. Med. 12 (2022) 1161.
[35] S. Kiratikanon, S.C. Chattipakorn, N. Chattipakorn, S. Kumfu, The regulatory effects of PTPN6 on inflammatory process: reports from Mice to Men, Arch. Biochem. Biophys. 721 (2022) 109189.
[36] X. Zhang, J. Chen, M. Zhang, S. Liu, T. Wang, T. Wu, B. Li, S. Zhao, H. Wang, L. Li, Single-cell and bulk sequencing analyses reveal the immune suppressive role of PTPN6 in glioblastoma, Aging (Albany NY) 15 (2023) 9822.
[37] Y. Song, X. Ma, M. Zhang, M. Wang, G. Wang, Y. Ye, W. Xia, Ezrin mediates invasion and metastasis in tumorigenesis: a review, Front. Cell. Dev. Biol. 8 (2020) 588801.
[38] H. Osawa, C.A. Smith, Y.S. Ra, P. Kongkham, J.T. Rutka, The role of the membrane cytoskeleton cross-linker ezrin in medulloblastoma cells, Neuro Oncol. 11 (2009) 381–393.
[39] Z. Chen, R.M. Ioris, S. Richardson, A.N. Van Ess, I. Vendrell, B.M. Kessler, F.M. Buffa, L. Busino, S.C. Clifford, A.N. Bullock, Disease-associated KBTBD4 mutations in medulloblastoma elicit neomorphic ubiquitylation activity to promote CoREST degradation, Cell Death Differ. (2022) 1–15.
[40] G. Robinson, M. Parker, T.A. Kranenburg, C. Lu, X. Chen, L. Ding, T.N. Phoenix, E. Hedlund, L. Wei, X. Zhu, Novel mutations target distinct subgroups of medulloblastoma, Nature 488 (2012) 43–48.
[41] Y. Sun, L. Wang, X. Xu, P. Han, J. Wu, X. Tian, M. Li, FOXO4 inhibits the migration and metastasis of colorectal cancer by regulating the APC2/β-catenin axis, Front. Cell. Dev. Biol. 9 (2021) 659731.
[42] M.A. Kreus, S.T. Lehtonen, J.M. Mäkinen, H.E. Lappi-Blanco, K.E.M. Laitakari, S.A. Johnson, R.M.L. Hinttala, R.L. Kaarteenaho, High NHLRC2 expression Is associated with shortened survival in lung adenocarcinoma, Transl. Lung Cancer Res. 12 (2023) 1221.
[43] H. Xu, J. Liu, Y. Zhang, Y. Zhou, L. Zhang, J. Kang, C. Ning, Z. He, S. Song, KIF23, under regulation by androgen receptor, contributes to nasopharyngeal carcinoma deterioration by activating the Wnt/β-catenin signaling pathway, Funct. Integr. Genomics 23 (2023) 116.
[44] H. Ni, D. Ji, Z. Huang, J. Li, SMAGP knockdown inhibits the malignant phenotypes of glioblastoma cells by inactivating the PI3K/Akt pathway, Arch. Biochem. Biophys. 695 (2020) 108628.
[45] S.M. Afify, G. Hassan, A. Seno, M. Seno, Cancer-inducing niche: the force of chronic inflammation, Br. J. Cancer. 127 (2022) 193–201.
[46] U. Basak, T. Sarkar, S. Mukherjee, S. Chakraborty, A. Dutta, S. Dutta, D. Nayak, S. Kaushik, T. Das, G. Sa, Tumor-associated Macrophages: an Effective Player of the Tumor Microenvironment, Front Immunol. 14 (2023) 1295257.